

HI holes in galactic disks: Tracing the dark matter distribution

E. I. Vorobyov¹ and Yu. A. Shchekinov²

¹ Institute of Physics, Stachki 194, Rostov-on-Don, Russia and Isaac Newton Institute of Chile, Rostov-on-Don Branch

e-mail: eduard_vorobev@mail.ru

² Department of Physics, University of Rostov, and Isaac Newton Institute of Chile, Rostov-on-Don Branch, Rostov-on-Don, 344090 Russia

e-mail: yus@phys.rsu.ru

Abstract. Multiple SN explosions in disk galaxies efficiently evacuate gas and form cavities with the sizes and shapes of the surrounding envelopes determined by the total amount of injected energy and by the initial gas distribution. Such cavities are seen as HI holes when observed in face-on galaxies. Gas hydrodynamics simulations are performed to obtain the quantitative characteristics of HI holes that could serve for the determination of the gas vertical scale height and the corresponding dark matter content and its distribution. Among these characteristics is the ratio of the maximum column density in the HI ring surrounding the hole to the background HI column density and the vertical expansion velocity of gas in the HI ring. We show that in some cases the extragalactic background ionizing radiation may produce HI holes in the outer regions of galaxies, and can account for the existence of HI holes in nearby face-on galaxies with the apparent lack of an underlying stellar population.

Key words. ISM: supernova remnants – ISM: bubbles

1. Introduction

The interstellar medium (ISM) shaped by the energy release from exploding massive stars provides the best sample for studying star formation processes on a “microscopic” level. The diversity of HI structures and associated H α distributions discovered in our own and nearby galaxies shows that star formation processes and dynamics of interaction of massive stars with the ISM are strongly environmentally dependent. Prominent examples are found in the Milky Way (Heiles 1984), M31 (Brinks 1981, Brinks & Bajaja 1986), M33 (Deul & den Hartog 1990), Holmberg II (Puche et al. 1992), NGC 891 (Dettmar & Schulz 1992), M101 and NGC 6946 (Kamphuis 1993), NGC 253 (Sofue, Wakamatsu & Malin 1994), SMC (Staveland-Smith et al. 1997) and LMC (Kim et al. 1999), IC 10 (Wilcots & Miller 1998), IC 2574 (Walter & Brinks 1999), Holmberg I (Ott et al. 2001), and others. Edge-on (such as NGC 891, NGC 4631, NGC 253) and face-on (such as Holmberg I and II, IC 2574, SMC and LMC) galaxies show these “microscopic” structures in vertical and horizontal directions, respectively, and develop our understanding of not only the interrelation between the observed HI/H α structures and star formation activity (Dettmar 1992, Rand 1996, Sofue, Wakamatsu & Malin 1994, Rossa & Dettmar 2003,

Stewart et al. 2000, Walter & Brinks 1999), but also the factors governing the star formation process itself.

Among these factors, the dark matter distribution in radial and vertical directions is of principle importance. At the same time, the influence of the dark matter distribution on the dynamics of HI and H α structures in edge-on and face-on galaxies was left aside general discussion. Only recently Ott et al. (2001) paid closer attention to the relevance of HI dynamics in the dwarf irregular galaxy Holmberg I to the vertical gas distribution. However, available estimates of the vertical scale heights are still based on qualitative arguments and assumptions on the contribution of the dark matter to the total gravitational potential. In this paper we address the question of whether the observations of morphologies and quantitative characteristics of the HI holes in face-on galaxies can provide us with firm conclusions about the vertical scale height of the HI distribution. For this purpose, we study numerically the characteristics of HI flows associated with multiple SN explosions. We determine the dependence of these characteristics on the vertical scale height of the HI distribution and, consequently, on the vertical shape of the gravitational potential and dark matter distribution.

The paper is organized as follows. In Sect. 2 the numerical model is formulated, and the quantitative characteristics of HI holes are numerically investigated for different vertical scale heights of gas distribution in face-on galax-

Table 1. Model parameters

h^\dagger	ρ_{d0}	r_0	ρ_*	h_*	v_*	M_d
0.5	0.07	0.227	0.02	0.3	7	8×10^7
0.37	0.015	2.26	0.02	0.3	7	3.7×10^8
0.21	0.13	1.5	0.03	0.3	8.5	2.2×10^9

[†] all scales are in kpc, densities in $M_\odot \text{ pc}^{-3}$, stellar velocity dispersion (v_*) in km s^{-1} , the mass of the dark matter (M_d) in M_\odot is computed within the radius of 2 kpc.

ies. In Sect. 3 the influence of the extragalactic background ionizing radiation on the vertical shape of the HI distribution is discussed. The main results are summarized in Sect. 4.

2. SNe driven supershells: dynamics and morphology

2.1. Model

The equilibrium HI distribution is obtained by solving the steady-state momentum equation in cylindrical (r, z) coordinates in a fixed gravitational potential determined by the stellar and dark matter components. The self-gravity of gas is neglected. The dark matter density distribution (ρ_d) is assumed to be that of a modified isothermal sphere (Binney & Tremaine 1987)

$$\rho_d = \frac{\rho_{d0}}{(1 + r/r_0)^2}, \quad (1)$$

where r is the radial distance from the galactic center, ρ_{d0} is the central density, and r_0 is the characteristic scale length. The stellar component is assumed to be vertically stratified (Spitzer 1942)

$$\rho_* = \rho_{*0} \text{sech}^2(z/h_*), \quad (2)$$

where ρ_* is the stellar density, ρ_{*0} is the stellar midplane density, and h_* is the vertical scale height of stellar distribution.

The resulting equilibrium HI distribution is distinct for different dark matter and stellar distributions. Its vertical shape is neither Gaussian nor exponential (Celnik et al. 1979), however, it is better fitted by a Gaussian than by an exponent. We consider three different models with three different gas vertical scale heights. The parameters of the stellar and dark matter distributions for each model are shown in Table 1. Fitting the equilibrium vertical HI distribution of each model by a Gaussian, we obtain the 1σ gas scale heights of $h=210, 370,$ and 500 pc at the galactocentric radius of 2 kpc. For comparison, the corresponding exponential gas scale heights are $h_{\text{exp}}=230, 400,$ and 540 pc, respectively.

Further, we assume that the size of SN-driven shells is much smaller than that of a galaxy. The radial dependence

of the dark matter gravitational potential within the shell can therefore be neglected and the initial equilibrium configuration of gas becomes a function of only the distance above the midplane of a galaxy. In all models the initial gas velocity dispersion was taken as $v_g = 9 \text{ km s}^{-1}$.

The energy of supernova explosions is released in a sphere with a radius of four zones. We use the constant wind approximation described in detail in Mac Low & Ferrara (1999). We convert the energy of each SN explosion (10^{51} ergs) totally into the thermal energy, because in the present simulations we deal with large stellar clusters capable of producing a hundred supernovae. With such a number of SN explosions, the surrounding ISM will be quickly heated and diluted, making radiative cooling within the injection sphere ineffective. We choose the energy input phase to last for 30 Myr, which roughly corresponds to a difference in the lifetimes of the most and least massive stars capable of producing SNe in a cluster of simultaneously born stars.

SNe generate a supersonically expanding wind that compresses the gas, thus creating a bubble filled with the hot ejected gas surrounded by a shell of compressed cold material. The gas dynamics is followed by solving the usual set of hydrodynamical equations in cylindrical coordinates using the method of finite-differences with a time-explicit, operator split solution procedure of the ZEUS-2D numerical hydrodynamics code described in detail in Stone & Norman (1992). We have implemented the cooling curve of Böhringer & Hensler (1989) for a metallicity of one tenth of solar. We use an empirical heating function tuned to balance the cooling in the background atmosphere so that it maintains the gas in hydrostatic equilibrium and may be thought of as a crude model for the stellar energy input. Cooling and heating are treated numerically using Newton-Raphson iterations, supplemented by a bisection algorithm for occasional zones where the Newton-Raphson method does not converge. In order to monitor accuracy, the total change in the internal energy density in one time step is kept below 15%. If this condition is not met, the time step is reduced and a solution is again sought.

2.2. Qualitative description

At the initial stages the remnant comes into a radiative phase relatively early, approximately at

$$t_r \sim 10^5 \left(\frac{L_{38}}{n} \right)^{1/2} \text{ yr}, \quad (3)$$

when its radius is only

$$R \sim 25 \left(\frac{L_{38}}{n} \right)^{1/2} \text{ pc}, \quad (4)$$

where L_{38} is the mechanical luminosity in $10^{38} \text{ ergs s}^{-1}$ released by multiple SN explosions, n is the ambient volume density. This implies that the remnant is always radiative before it expands out to $R \sim 2h$ and enters a breakthrough phase (i.e. the shell breaking out of the disk and

losing metal-enriched material to the intergalactic space). The breakthrough occurs at approximately

$$t \sim 10^{-3} \left(\frac{n}{L_{38}} \right)^{3/2} h^4 \text{ yr}, \quad (5)$$

where h is in parsecs. The further evolution shows a very fast drop of pressure inside the hot remnant and the “snowplow” expansion of a quasi-cylindrical shell of compressed cold material in the disk. Due to a sharp drop of pressure inside the remnant the expanding shell starts thickening and can no longer be treated as a thin shell. Figure 1a shows the temporal evolution of the inner and outer radii of the shell expanding in a face-on galaxy with a gas scale height of $h = 500$ pc and HI surface density of $\Sigma_{\text{HI}} = 10.7 M_{\odot} \text{ pc}^{-2}$. The surface density of the swept-up gas is generally not constant across the shell, it reaches a maximum near the outer edge of the shell and falls off on both sides. We define the inner radius of the shell as a radial distance where Σ_{HI} drops to its unperturbed value in the inner side of the shell. The outer radius is defined in the same manner. The mean radius is then obtained as an arithmetic average of the inner and outer radii. The mechanical luminosity of $L_{38} = 1$ is assumed, which is equivalent to 100 SN explosions during the first 30 Myr. The cooling rate for $T \geq 10^4$ K is taken from Böhringer & Hensler (1989), for $T < 10^4$ K the cooling function rapidly declines to zero. It is seen that the shell remains thinner than a quarter or less of its mean radius only in the SN-driven expansion phase during the first 30-35 Myr. At this evolutionary stage, the mean radius of the shell is well described by the $R \propto (L/\rho)^{1/5} t^{3/5}$ law (Castor et al. 1975) plotted by the dotted line in Fig. 1a, where $\rho = 0.5 \rho_0$ and ρ_0 is the midplane mass density of the ambient gas. The shell grows very fast after $t = 35$ Myr when a breakthrough is to occur. At the time of a breakthrough, the mean radius of the shell is $R \approx 1.6 h$. After the breakthrough the shell enters the “snowplow” phase and its mean radius grows approximately as $R \propto t^{1/3}$ (as shown in Fig. 1a by the dotted line).

In case of a smaller gas scale height ($h = 210$ pc), the breakthrough occurs at $t=13.5$ Myr when $R \approx 1.8 h$. The mean radius of the shell is poorly described by both the spherical ($R \propto t^{1/4}$, McCray & Kafatos 1987) and cylindrical ($R \propto t^{1/3}$) thin-shell “snowplow” expansion laws as shown in Fig. 1b by the dashed and dotted lines, respectively. Thus, it is obvious that when an HI hole seen in face-on galaxies is fitted by the spherical thin-shell “snowplow” expansion law $R \sim t^{1/4}$, the resultant energy input into the hole from SN explosions may be largely overestimated.

2.3. Dynamics versus vertical gas scale height

At the early expansion stages, when the shells remain nearly spherical, their kinematical and dynamical characteristics scaled to the proper mechanical luminosity and local density are similar in different environments (see

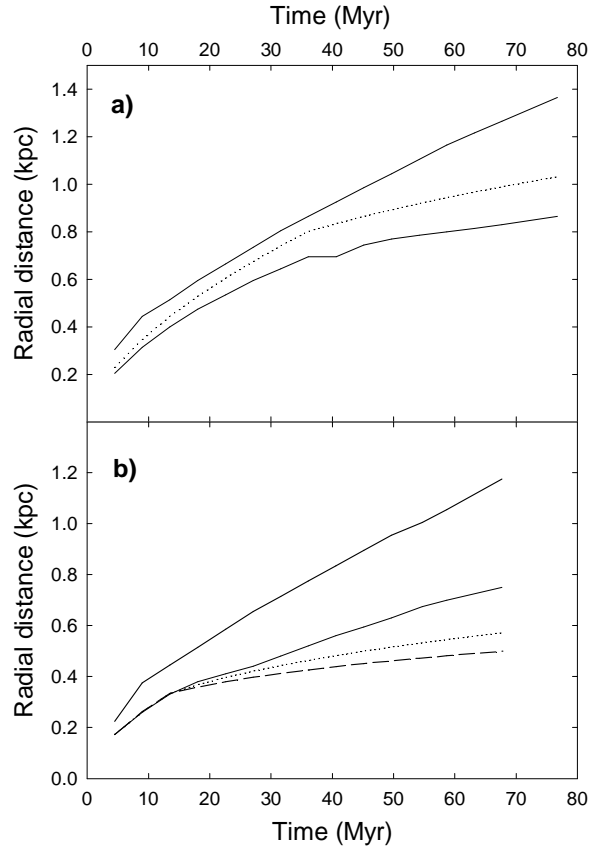


Fig. 1. **a)** The solid lines delineate the inner and outer radii of the shell expanding in a galaxy with $h = 500$ pc. The dotted line gives the radius of the shell as predicted from the $R \propto (L/\rho)^{1/5} t^{3/5}$ law for the SN-driven expansion at $t < 35$ Myr (Castor et al. 1975) and from the $R \propto t^{1/3}$ law for the “snow-plow” expansion at $t > 35$ Myr. **b)** The same for $h = 210$ pc. The dotted line gives the radius of the shell as predicted from the $R \propto t^{1/3}$ law for a cylindrical “snowplow” expansion at $t > 13.5$ Myr, the dashed line shows a spherical “snowplow” $R \propto t^{1/4}$ expansion.

discussion in Castor et al. 1975). Therefore, one should explore the later expansion stages in order to determine the large scale properties of a parent galaxy. At the later stages, the expanding shells are radiative and their expansion velocities are only weakly supersonic so that the corresponding Mach number is $M \gtrsim 1$ (in most face-on galaxies the expanding HI shells are marginally supersonic, or even subsonic as in the case of Holmberg II, see discussion in Shchekinov et al. 2001). In such conditions the compression factor of gas inside the shells (mass density contrast) is not high: for isothermal shock waves it is $\rho/\rho_0 = \gamma M^2$, where γ is the ratio of specific heats, and for weakly supersonic shocks at the later stages ($t \sim 30 - 40$ Myr) it can be around γ .

A directly observed quantity is the HI column density. For an HI hole in a face-on galaxy created by consecutive SN explosions, the HI column density in a ring of compressed gas surrounding the hole is

$$N(\text{HI}) \simeq \frac{2\sqrt{2}}{3} \frac{R^{3/2} n_0}{\sqrt{\Delta R}}, \quad (6)$$

where R is the ring radius, ΔR is its thickness, n_0 is the midplane density of ambient gas $n_0 = N_0(\text{HI})/h$, $N_0(\text{HI})$ is the column density of the background (unperturbed) HI gas. Substituting $\Delta R = R \rho_0/3\rho$ and $\rho/\rho_0 \sim \gamma$ into Eq. (6), one obtains a linear dependence of the relative HI column density on its radius in a face-on ring

$$\mathcal{K}_{\text{HI}} \equiv \frac{N(\text{HI})}{N_0(\text{HI})} \simeq 2 \frac{R}{h}, \quad (7)$$

with the slope inversely proportional to the HI vertical scale height of a parent galaxy. The highest relative column density \mathcal{K}_{HI} is reached when the breakthrough occurs at $R \sim \alpha h$, where α is a slowly varying function of the vertical gas scale height. Simulations in Sect. 2.2 indicate that $\alpha \approx 1.6$ for $h = 500$ pc, while for $h = 210$ pc $\alpha \approx 1.8$. An expanding ring reaches maximal relative column density $\mathcal{K}_{\text{HI}} \sim 4$ only in galaxies with rather low vertical scale heights $h \leq 200$ pc, where the compressed shell always remains supersonic. After the breakthrough, the compressed gas in the shell starts to move into the cavity because of a sharp drop in pressure, and the column density in the ring decreases approximately as $\propto R^{-1}$.

When the gas scale height is sufficiently large, the shell expansion becomes sonic before breaking out of the disk, the associated perturbation propagates with the sound speed and simultaneously the shell itself starts swelling into the cavity, which results in a decrease of the gas column density. This occurs when

$$R \simeq 230 L_{38}^{1/2} h_{100}^{1/2} \Sigma_{10}^{-1/2} \text{ pc}, \quad (8)$$

where $h_{100} = h/100$ pc, Σ_{10} is the unperturbed surface density of gas (Σ_{g0}) in units of $10 M_\odot \text{ pc}^{-2}$. For instance, when the gas scale height is $h = 500$ pc and the unperturbed surface density $\Sigma_{g0} = 10.5 M_\odot \text{ pc}^{-2}$, the shell becomes sonic when its radius is $R \simeq 500$ pc. As a consequence, the shell starts swelling into the cavity and the corresponding relative column density of the ring decreases.

Figure 2 shows the relative column density in the ring, \mathcal{K}_{HI} , obtained in our numerical simulations for three different vertical gas scale heights and two values of the undisturbed surface density Σ_{g0} . The curves exhibit the characteristic behaviour described above, with the maximal values of \mathcal{K}_{HI} being higher for the lower vertical gas scale heights. Specifically, for $h = 210$ pc the maximum value of \mathcal{K}_{HI} is approximately 3.4 at the time when the shell starts swelling because of a sharp pressure drop after the breakthrough. For larger h the maximum value of \mathcal{K}_{HI} is smaller. Note that \mathcal{K}_{HI} is virtually independent of Σ_{g0} . For the total period of energy injection ≤ 30 Myr and for the

vertical gas scale heights < 600 pc, the maximum value of \mathcal{K}_{HI} and the corresponding radius of a shell do not depend on the luminosity L , while in gaseous disks with $h \geq 600$ pc the maximum value of \mathcal{K}_{HI} and the corresponding radius scale as $L^{1/2}$. However, since a widely accepted value for the mechanical luminosity $L = 10^{38} \text{ ergs s}^{-1}$ is typical for OB associations with a Salpeter IMF, one may expect that the curves depicted in Fig. 2 represent a universal relation and may be used to draw firm conclusions about the vertical scale heights of HI distributions in disk galaxies. It is obviously seen that the \mathcal{K}_{HI} versus R relation is characteristic for each vertical gas scale height only in the early phases when the shell has not yet broken out of the disk, while after the breakthrough \mathcal{K}_{HI} can barely be distinguished among different h . Note in Fig. 2 a range in which the relative column density in the ring varies in galaxies with low vertical gas scale heights. It is 1.4-3.4 for $h = 210$ pc, while \mathcal{K}_{HI} is restricted to a narrower range of 1.3-2 in galaxies with $h = 700$ pc. Thus, a narrow spread of observed column densities may indirectly indicate that the vertical gas scale height is large. Moreover, considering a universal and single-valued dependence of $\mathcal{K}_{\text{HI}}(h, R)$ for $R \leq 600 - 700$ pc, the local gas scale height h can be inferred directly from the measurements of \mathcal{K}_{HI} . Further, the measurements of \mathcal{K}_{HI} for the individual HI holes located at different galactocentric distances allow for the determination of the radial variations in the gas scale height.

The increase in the mass of the dark matter generally makes a gas disk thinner, i.e. the gas scale height h decreases as the dark matter mass increases. Assuming the *local* plane-parallel gas distribution, the total density $\rho_{\text{tot}}(0, r)$ in the disk at the galactocentric radius r and $z = 0$ can be derived from $h(r) = v_g / \sqrt{4\pi G \rho_{\text{tot}}(0, r)}$ (van der Kruit 1981). Provided that the radial distribution of the visible mass is known from independent measurements, one can obtain the radial distribution of the dark matter in the galactic plane. These are, of course, very approximate estimates; nevertheless, a similar approach applied to the dwarf irregular galaxy Holmberg I by Ott et al. (2001) has yielded a dark matter mass within the HI content of the galaxy, the value of which is in agreement with that obtained in a more sophisticated numerical modeling by Vorobyov et al. (2004). Note, however, that the flaring and warping of the gas disk may further complicate this analysis.

The velocity field of a shell expanding in a nearly face-on galaxy can additionally hint at the vertical structure of gas. At the initial stages far from breakthrough, the vertical component of gas velocity in an expanding shell, v_z , scales as $\sqrt{1 - (r/R)^2}$, where r is the projected distance from the geometrical center of a shell and R is the shell radius. However, when the shell is near breakthrough, a substantial amount of gas constituting the shell becomes involved in strong vertical motion. In Fig. 3 we plot the mass-weighted v_z as a function of the projected distance from the geometrical center of a shell for different vertical gas scale heights and different fixed shell radii. The solid lines represent the shells with a radius of $R = 0.5$ kpc,

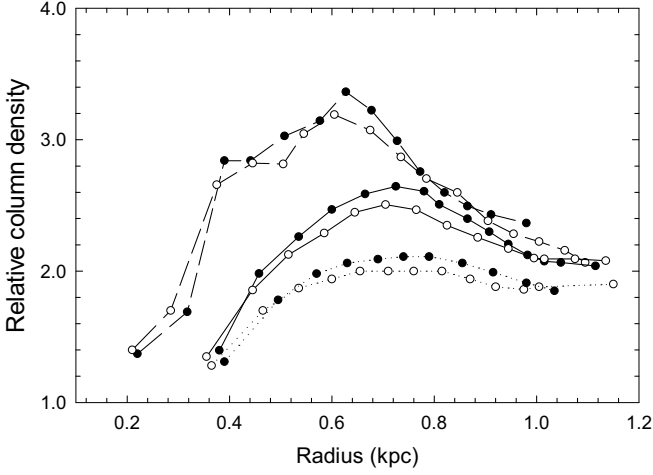


Fig. 2. Relative column density in the ring versus its radius: dashed, solid, and dotted lines represent $h = 210$, 500 , and 700 pc, respectively; open circles correspond to $\Sigma_{g0} = 15.2 M_{\odot} \text{pc}^{-2}$, filled circles – $\Sigma_{g0} = 10.7 M_{\odot} \text{pc}^{-2}$.

while the dotted lines correspond to the shells with a radius of $R = 0.7$ kpc.

It is seen that the expanding gas is only weakly supersonic (the corresponding Mach number of 2-3) in the shells that are at the early phases of expansion, well before breakthrough ($R = 0.5$ kpc, $h = 370$ and 500 pc). On the other hand, the shell that approaches the breakthrough phase ($R = 0.5$ kpc and $h = 210$ pc) shows a steep velocity increase up to $v_z = 60 \text{ km s}^{-1}$ at the inner edge of the projected shell. The v_z radial profiles remain qualitatively similar at different phases of the shell expansion, namely at $R = 0.5$ kpc and $R = 0.7$ kpc.

At the breakthrough phase, the radius of a shell is almost twice as large as the gas scale height h . From this point of view, one may expect that the most extended HI holes in face-on galaxies (such as HI holes number 2, 5, 8, 10 and others in Holmberg II, Puche et al. 1992) whose z -velocity reveals such a behaviour at the inner edges can provide us with a direct measure of the local gas scale height. Specifically, scanning the HI radial velocity profiles within a hole with a beam smaller than its size (for the Ho II case, the beam must be less than $4'' - 6''$) could help to identify nearly breaking-through shells, the radii of which could then serve as a direct measure of the local gas scale height.

Out-of-plane SN explosions in nearly face-on galaxies can also provide quite a robust tool for the determination of the gas vertical scale height. In Fig. 4 we plot typical HI spectra of the shells produced by 100 successive SNe located at 100 pc above the midplane. The HI spectrum

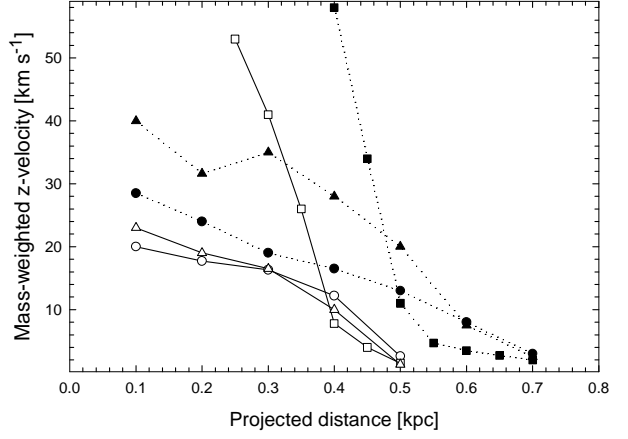


Fig. 3. Mass-weighted z -velocity profiles versus projected distance from the geometrical center of the shells. Solid and dotted lines represent the shells with the radii of 0.5 and 0.7 kpc, respectively. Open squares – $h = 210$ pc, $t = 18$ Myr; open triangles – $h = 370$ pc, $t = 13.5$ Myr; open circles – $h = 500$ pc, $t = 13.5$ Myr. Filled squares – $h = 210$ pc, $t = 36$ Myr; filled triangles – $h = 370$ pc, $t = 31$ Myr; filled circles – $h = 500$ pc, $t = 29$ Myr. The unperturbed HI surface density is $\Sigma_{g0} = 10.7 M_{\odot} \text{pc}^{-2}$.

is obtained for a 1 kpc diameter beam centered on the expanding shell. Two model galaxies with different gas scale heights are considered: $h = 500$ pc and $h = 210$ pc. A one-dimensional velocity dispersion of $\sigma_g = 3 \text{ km s}^{-1}$ is assumed for the gas forming an expanding shell when constructing the model HI spectra, while $\sigma_g = 9 \text{ km s}^{-1}$ is adopted for the unperturbed gas. The HI spectrum of the shell expanding in a galaxy with $h = 500$ pc is characterized by a typical two-humped structure. A smaller part of the accelerating shell expanding upwards ($v_z > 0$) and a more massive part of the shell expanding downwards ($v_z < 0$) with approximately constant velocity are clearly seen. The HI spectrum of the shell expanding in a galaxy with $h = 210$ pc has a single peak located at $v_z \neq 0$. Velocity centroids of gas expanding downwards are obviously smaller for lower gas scale heights h , because lower scale heights lead to a faster onset of breakthrough and, therefore, to a faster drop of pressure inside the SN-driven shell.

In Fig. 5 we plot the absolute values of the peak v_z velocities of gas expanding downwards as a function of the corresponding HI intensities (see Fig. 4) for three different gas scale heights: $h = 210$, 370 , and 500 pc. It is clearly seen that the smaller peak z -velocities are associated with the shells expanding in galaxies with lower gas scale heights. A distinguishing feature of this dependence is that the peak expansion velocity is virtually independent of intensity in a relatively wide range covering the lat-

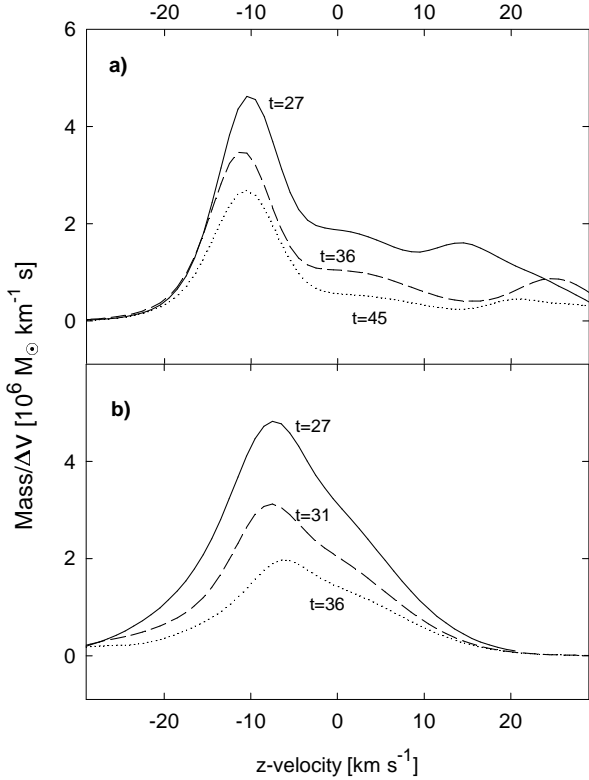


Fig. 4. The HI spectrum of an expanding shell produced by 100 successive SNe located 100 pc above the midplane in a galaxy with **a)** $h = 500$ pc, **b)** $h = 210$ pc. The HI spectra are numerically obtained for a 1 kpc diameter beam centered on the shell at three different times in Myr as indicated in each frame.

est stages of expansion before and after the breakthrough, and varies approximately as

$$v_z^{\text{peak}} \simeq 2 \left(\frac{h}{100 \text{ pc}} \right)^{0.9} \left(\frac{z_*}{100 \text{ pc}} \right)^{-0.24} \text{ km s}^{-1}. \quad (9)$$

where z_* is the location of SNe above the midplane.

3. Effects of external ionizing radiation

One of the most striking facts related to HI holes in dwarf face-on galaxies is the lack of an underlying stellar population that could produce a strong energy input into the ISM. This tendency is obviously seen in Holmberg II (Ho II) where most extended HI holes are located outside the stellar disk (Rhode et al. 1999, Stewart et al. 2000). Hence, the SN origin of those HI holes in Ho II is questionable. An alternative explanation of the HI hole formation connected with high-velocity HI clouds (HVCs) falling onto the disk seems to be excluded in the case of Ho II, because no HVCs are found nearby. In this case, Efremov et al. (1998) argue that a supernova in the merging event of a compact binary system may be responsible for HI hole creation. However, a distinguishing feature of

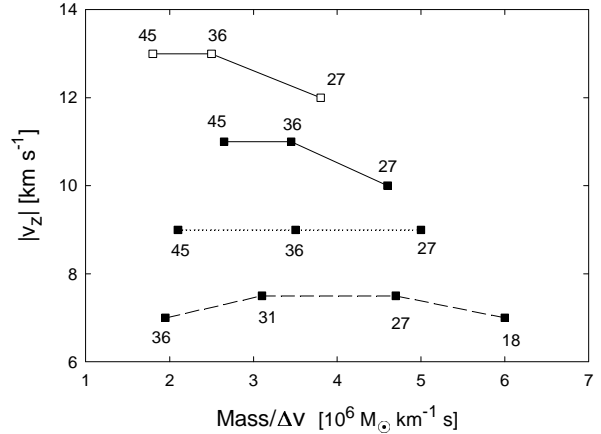


Fig. 5. The peak z -velocity versus HI intensity for different gas scale heights and locations of SN explosions above the midplane: dashed line – $h = 210$ pc, SNe at $z_* = 100$ pc; dotted line – $h = 370$ pc, SNe at $z_* = 100$ pc; solid line with filled squares – $h = 500$ pc, SNe at $z_* = 100$ pc; solid line with open squares – $h = 500$ pc, SNe at $z_* = 50$ pc. Different evolutionary stages of the shells are labeled in Myr.

multiple HI holes on the periphery of Ho II is that they form quite a regular structure resembling a spiral wave (see Stewart et al. 2000), and seem unlikely to be produced by regularly placed supernovae explosions. In this connection it is worth mentioning the role of an external ionizing radiation field in shaping the HI distribution, particularly on the galactic periphery.

The position of the boundary between HI and HII layers, z_i , in an exponential vertical gas distribution ionized by a given flux of external UV photons I is determined by the following equation $2\pi I = \alpha_r n_0^2 \int_{z_i}^{\infty} \exp(-2z/h) dz$. The observed column density of atomic hydrogen, $N(\text{HI}) = 2n_0 \int_0^{z_i} \exp(-z/h) dz$, can then be found as

$$N(\text{HI}) = N_0(\text{H}) - \sqrt{\frac{4\pi I h}{\alpha_r}}, \quad (10)$$

where α_r is the hydrogen recombination rate and $N_0(\text{H}) = 2n_0 h$ is the total column density of hydrogen (both neutral and ionized), n_0 is the total midplane density of hydrogen. It is readily seen that for a typical value of the background ionizing flux of $I \sim 10^6$ photons $\text{cm}^{-2} \text{s}^{-1} \text{sr}^{-1}$ and for $h \sim 300$ pc the column density of ionized hydrogen can reach $3 \times 10^{20} \text{ cm}^{-2}$, nearly coincident with the observed in Ho II at the radii of ~ 6 arcmin (Puche et al. 1992). This implies that the observed $N(\text{HI})$ may represent a small fraction of the total amount of hydrogen, and thus a relatively weak perturbation in n_0 and/or in $N_0(\text{H})$ can cause a rather strong variation in the amount of neutral hydrogen. This effect increases for a flaring gaseous disk

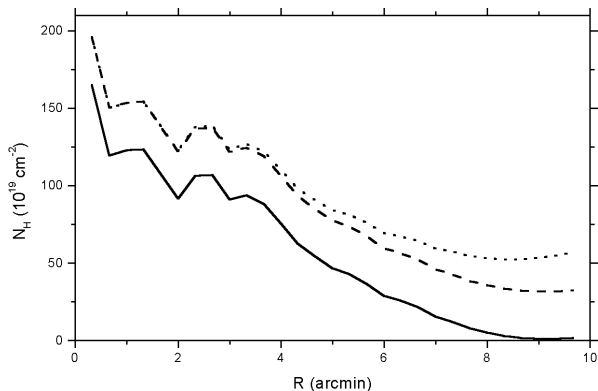


Fig. 6. Comparison of the total hydrogen column density and the observed HI in Ho II: solid line – observed HI (Puche et. al. 1992), dashed line shows total column density $N_0(\text{H})$ from (10) with $h = 625$ pc, dotted line – $N_0(\text{H})$ with $h = 625 + 18.6(R - 1)^2$.

with the scale height h growing outwards. In Fig. 6 we plot the total column density of hydrogen, $N_0(\text{H})$, as a function of Ho II radius. $N_0(\text{H})$ is derived from the observed column density of neutral hydrogen $N(\text{HI})$ for two models of the vertical gas distribution in Ho II: a plane-parallel distribution with $h=625$ pc and a flaring disk with $h = 625 + 18.6(R - 1)^2$ pc, where R is given in arcminutes. In the outer regions at $R \gtrsim 6$ arcmin, the observed $N(\text{HI})$ may represent a relatively small (less than 50 %) fraction of the total hydrogen content, and thus can be easily disturbed, ionized, and transformed into a hole of depleted HI column density.

In principle, HI holes created by multiple SN explosions can become radially asymmetric due to radial variations in the gas density, particularly at larger distances from the galactic center where the flaring of the gas disk may dominate. For an exponential disk with the density distribution $\rho \propto \exp(-z/h - R/R_0)$, the expansion velocity of a shell at a given point varies as $v_s \propto \exp(z/2h + R/2R_0)$. In this case, the geometrical center of an HI shell can be shifted outward with respect to the position of SN explosions (Kalberla, private communication). Typical scales in vertical and radial directions are of the order of hundreds and thousands of parsecs, respectively. For example, for the Ho II galaxy $h \sim 600$ pc, while the radial scale for the HI surface density $R_0 \sim 3$ kpc (Puche et al. 1992, Bureau & Carignan, 2002). For face-on galaxies, direct measurements of the radial distributions of the volume density or flaring are not available, but one can assume that the radial scale lengths for them are of the same order as for the HI surface density. The corresponding deviations of the expansion velocities in radial δv_R and vertical δv_z directions from a precise spherical

shape can be estimated then as $\delta v_R/\delta v_z \sim h/R_0 \ll 1$. In the case of Ho II, it becomes $\delta v_R/\delta v_z \sim 0.2$. Hence, one may conclude that the expected radial asymmetry of a shell, and the corresponding displacement of the geometrical center of a shell with respect to the location of SN explosions, is less than 20% of the gas scale height.

4. Summary

Clustered supernova explosions in the disk of a face-on galaxy produce an expanding shell of compressed material, which is seen as an HI ring surrounding a central HI depression. In this paper we show that several physical characteristics of expanding shells are sensitive to the gas scale height and, hence, can be used for the determination of the dark matter content in face-on disk galaxies.

- A functional dependence of the relative column density of gas in the HI ring (\mathcal{K}_{HI}) on the radius of the ring is found to be specific for a given gas scale height h , which makes it possible to infer h from observations of even a single HI ring. This is particularly true for the shells near breakthrough phase.

- The vertical component of gas velocity in an expanding shell reveals a characteristic behaviour (particularly, at the stages close to a breakthrough), which can be used to trace the gas scale height h in galaxies with a sufficiently thin HI layer.

- Out-of-plane SN explosions produce asymmetric expansion, with a more massive part of the shell propagating towards the denser regions of the disk. The velocity of this part of the shell is a single-valued function of the scale height h and the height above the midplane at which the SN explosions take place.

- Some of HI holes, particularly in the outer regions of a galaxy, can be connected to the ionization of HI layer by extragalactic UV photons.

Acknowledgments

We would like to thank the referee, Dr. P. M. W. Kalberla, for his suggestions and critical comments that substantially improved the paper. This work was supported by the RFBR (projects No 00-02-17689) and the INTAS grant YSF-2002-33. YS acknowledges financial support from *Deutsche Forschungsgemeinschaft, DFG* (project SFB N 591, TP A6).

References

- Böhringer, H., & Hensler, G. 1989, *A&A*, 215, 147
 Binney, J., & Tremaine, S. 1987, *Galactic Dynamics* (Princeton: Princeton Univ. Press)
 Brinks, E. 1981, *A&A*, 95, L1
 Brinks, E., & Bajaja, E. 1986, *A&A*, 169, 14
 Castor, J., McCray, R., Weaver, R., 1975, *ApJ*, 200, L107
 Celnik, W., Rohlfs, K., & Braunsfurth, E. 1979, *A&A*, 76, 24C
 Dettmar, R.-J., Schultz, H. 1992, *A&A*, 254, 25
 Dettmar, R.-J. 1992, *Fund. Cosm. Phys.*, 15, 143
 Deul, E. R., & den Hartog, R. H. 1990, *A&A*, 229, 362

- Efremov, Y. N., Elmegreen, B. G., & Hodge, P. W. 1998, *ApJ*, 501, L163
- Heiles, C. 1984, *ApJS*, 55, 585
- Kamphuis, J. J. 1993, Ph. D. thesis, Univ. Groningen
- Kim, S., Stavely-Smith, L., Dopita, M. A., Freeman, K. C., Sault, R. J., Kesteven, M. J., & McConnell, D. 1999, *ApJ*, 503, 729
- Mac Low, M.-M., & Ferrara, A. 1999, *ApJ*, 513, 142
- McCray, R., & Kafatos, M. 1987, *ApJ*, 317, 190
- Ott, J., Walter, F., Brinks, E., Van Dyk, S. D., Dirsch, B., & Klein, U. 2001, *AJ*, 122, 3070
- Puche, D., Westpfahl, D., Brinks, E., & Roy, J.-R. 1992, *AJ*, 103, 1841
- Rand, R. J. 1996, *ApJ*, 462, 712
- Rhode K. L., Saltzer J. J., Westpfahl D. J., Radice L. A. 1999, *AJ*, 118, 323
- Rossa, J. & Dettmar, R.-J. 2003, astro-ph/0304452
- Shchekinov Yu. A., Dettmar, R.-J., Schröer, A., & Steinacker, A. 2001, *Astron. Astroph. Transact.*, 20, 237
- Sofue, Y., Wakamatsu, K.-I., & Malin, D. F. 1994, *AJ*, 108, 2102
- Spitzer, L. 1942, *ApJ*, 95, 329
- Stavely-Smith, L., Sault, R. J., Hatyidimitrou, D., Kesteven, M. J., & McConnell, D. 1997, *MNRAS*, 289, 225
- Stewart, S. G., Fanelli, M. N., Byrd, G. G., Hill, J. K., Westpfahl, D. J., Cheng, K.-P., O'Connell, R. W., & Roberts, M. S. 2000, *ApJ*, 529, 201
- Stone, J. M., & Norman, M. L. 1992, *ApJS*, 80, 753
- van der Kruit, P. C. 1981, *A&A*, 99, 298
- Vorobyov, E. I., Klein, U., Shchekinov, Yu. A., & Ott, J. 2004, *A&A*, in press
- Walter, F., & Brinks., E. 1999, *AJ*, 118, 273
- Wilcots, E. M., & Miller, B. W. 1998, *AJ*, 116, 2363